Journal of Colloid and Interface Science 405 (2013) 85–95

Contents lists available at SciVerse ScienceDirect

Journal of Colloid and Interface Science

www.elsevier.com/locate/jcis

Influence of drying method on the surface energy of cellulose nanofibrils determined by inverse gas chromatography

Yucheng Peng [a,b], Douglas J. Gardner [a,b,*], Yousoo Han [a,b], Zhiyong Cai [c], Mandla A. Tshabalala [c]

[a] Advanced Structures and Composites Center, University of Maine, 35 Flagstaff Road, Orono, ME 04469, USA
[b] School of Forest Resources, University of Maine, 35 Flagstaff Road, Orono, ME 04469, USA
[c] Forest Products Laboratory, USDA Forest Service, One Gifford Pinchot Drive, Madison, WI 53726-2398, USA

ARTICLE INFO

Article history:
Received 17 April 2013
Accepted 15 May 2013
Available online 30 May 2013

Keywords:
Cellulose nanofibrils
Drying
Surface energy
Inverse gas chromatography

ABSTRACT

Research and development of the renewable nanomaterial cellulose nanofibrils (CNFs) has received considerable attention. The effect of drying on the surface energy of CNFs was investigated. Samples of nanofibrillated cellulose (NFC) and cellulose nanocrystals (CNC) were each subjected to four separate drying methods: air-drying, freeze-drying, spray-drying, and supercritical-drying. The surface morphology of the dried CNFs was examined using a scanning electron microscope. The surface energy of the dried CNFs was determined using inverse gas chromatography at infinite dilution and column temperatures: 30, 40, 50, 55, and 60 °C. Surface energy measurements of supercritical-dried NFCs were performed also at column temperatures: 70, 75, and 80 °C. Different drying methods produced CNFs with different morphologies which in turn significantly influenced their surface energy. Supercritical-drying resulted in NFCs having a dispersion component of surface energy of 98.3 ± 5.8 mJ/m^2 at 30 °C. The dispersion component of surface energy of freeze-dried NFCs (44.3 ± 0.4 mJ/m^2 at 30 °C) and CNCs (46.5 ± 0.9 mJ/m^2 at 30 °C) were the lowest among all the CNFs. The pre-freezing treatment during the freeze-drying process is hypothesized to have a major impact on the dispersion component of surface energy of the CNFs. The acid and base parameters of all the dried CNFs were amphoteric (acidic and basic) although predominantly basic in nature.

1. Introduction

Cellulose, as the most abundant biopolymer in nature, is the most influential material in the history of human culture. Its applications are diverse, and include housing, paper and textiles, pharmaceuticals, and chemicals [1–4]. Cellulose is the primary structural building block of trees and other plants and can be economically extracted from woody fibers. Regardless of its source, cellulose can be characterized as a high molecular weight linear syndiotactic homopolymer composed of D-anhydroglucopyranose units (AGU) which are linked together by β-(1 → 4)-glycosidic bonds [1]. In woody plants, cellulose linear chains aggregate to highly ordered structures referred to as nanofibrils or elementary fibrils. These nanofibrils of cellulose are then packed into larger units to form microfibrils which in turn are assembled into cellulose fibers such as the pulp fibers. Nanofibrils in the woody plant are nano-scale fibers with average cross-sectional dimensions of about 10 nm × 3.5 nm. They consist of crystalline and amorphous domains with cellulose chains parallel to the nanofibril axis [5–7]. Nanofibrils are generally produced from wood fiber, plant fiber, pulp fiber, microcrystalline cellulose (MCC), and microfibrillated cellulose (MFC) using mechanical or chemical methods. Processing dilute slurries of cellulose fibers, including wood fiber, plant fiber, and pulp fiber, by grinding or high-pressure homogenizing action produces nanofibrillated cellulose (NFC) [2,4,8], while digestion of amorphous cellulosic domains of the raw materials through an acid hydrolysis process produces cellulose nanocrystals (CNC) [4,9]. During the mechanical fibrillation process, the treatment of the raw materials via oxidation mediated by 2,2,6,6-tetramethylpiperidine-1-oxyl (TEMPO) radical facilitates the disintegration of the materials into individual nanofibrils [4,10]. These nanofibrils are referred to as TEMPO-oxidated NFCs. NFC can also be utilized as a raw material for producing CNC. These CNC and NFC suspensions, which are denoted as cellulose nanofibril (CNF) suspensions in this study, are produced on the pilot scale and are commercially available in US, Europe, and Japan [4,11–13]. A comprehensive review of the manufacturing processes for NFC and CNC was reported by Dufresne [4].

With the availability of CNF suspensions in pilot-scale quantities, great opportunities are available for exploring their novel applications, such as the utilization of CNFs as nano-fillers to reinforce polymers in the plastics industry [2,14,15] and as novel tablet

* Corresponding author at: Advanced Structures and Composites Center, University of Maine, 35 Flagstaff Road, Orono, ME 04469, USA. Fax: +1 207 581 2074.
E-mail address: douglasg@maine.edu (D.J. Gardner).

0021-9797/$ - see front matter © 2013 Elsevier Inc. All rights reserved.
http://dx.doi.org/10.1016/j.jcis.2013.05.033

excipients in the pharmaceutical industry [3,16]. For these applications, drying CNF suspension is a prerequisite. A detailed study of drying CNF suspensions was conducted by Peng et al. [17–19]. The CNF suspensions, including NFC and CNC suspensions, were each dried by: air-drying (or oven drying), freeze-drying, spray-drying, or supercritical-drying. After drying, CNFs with various morphologies, crystalline structures, residue moisture contents, and thermal stabilities were produced [17,19]. Knowledge of both the nature and magnitude of surface energetics of these dried CNFs is critical in optimizing the process of manufacturing CNF-reinforced polymer nanocomposites with desirable properties. The properties of CNF-reinforced polymer nanocomposites are controlled mainly by: (1) agglomeration of cellulose fibers, (2) interactions between cellulose and the polymer, (3) wetting of cellulose fibers, and (4) the distribution and dispersion of cellulose fibers within the polymer matrix. These four properties are directly determined by surface energetics of dried CNFs. Surface energy measurements are also critical for using CNFs in pharmaceutical formulations, especially in the prediction of drug adsorption, cohesion, adhesion, mucoadhesion, dispersion stability, coating performance and lubricant sensitivity [3,20].

The surface energetics of cellulosic materials have been investigated intensively using several different techniques: contact angle analysis of cellulose films, powder contact angle analysis, the Wilhelmy technique, thin-layer wicking, inverse gas chromatography, etc. [7]. The surface energy data of various cellulose materials were summarized by Gardner et al. [7]. Among these techniques, inverse gas chromatography (IGC) is one of the most widely used methods and has been successfully employed for characterizing the surface energies of cellulosic materials [20–35]. Cellulosic materials for different applications were investigated in the mentioned research work: (1) microcrystalline cellulose (MCC) for pharmaceutical formulations [20], (2) pulp fibers for paper [23,30], and (3) cotton fibers for the textile industry [35]. The most relevant studies cover cellulosic fibers for manufacturing polymer composites [28,29,31]. As cellulose is a highly hydrophilic natural material, its incorporation into a polymeric matrix should be carried out in such a way as to avoid the uptake of water from the environment. At the same time, compatibility between the surfaces of these fibers and that of polymers must be optimized for the improvement of material performance. When cellulose fiber is used in a polyolefin-based matrix, the interactions between the fiber and the matrix are dominated by the ubiquitous Lifshitz-van der Waals (dispersion) forces. However, when cellulose is compounded with hydrophilic matrices, the Lewis acid–base (specific) interactions must also be evaluated. Generally, the surface of cellulosic materials is categorized as amphoteric [23,30,31]. However, Jacob and Berg [23] indicated that the solid surfaces of cellulose are predominantly acidic while other research results show higher basicity on cellulose surfaces [30,31]. The research work conducted by Dorris and Gray [21] showed that the dispersion component (γ^{LW}) of surface energy was (1) 49.9 mJ/m^2 for cotton cellulose at 40 °C and (2) 38.8 mJ/m^2 for thermomechanical pulp fibers (TMP) at 30 °C. The measurement of the dispersion component of two MCC samples (Emcocel 50 M and Emcocel HD 90) using IGC was also conducted [20] at 30 °C and 0% relative humidity (RH) and the results were 55.5 (0.6) and 45.6 (0.4) mJ/m^2. The authors attributed the lower dispersion component of surface energy of Emcocel HD 90 to its higher density compared with Emcocel 50 M. Increased RH decreases the dispersion component of surface energy [20,29]. Different material sources were also observed to cause significant differences in the dispersion component of surface energy. The dispersion component of surface energy of 14 different cellulosic fibers was examined using IGC and the results indicated that they differ within a range from 35.5 to 44.2 mJ/m^2 [32]. Crystallinity also affects the dispersion component of surface energy. Belgacem et al. [36] demonstrated that MCC has a significantly higher dispersion component of surface energy (41.0 mJ/m^2) than that of amorphous cellulose (27.4 mJ/m^2).

For CNFs produced by homogenization or acid hydrolysis processes, the surface properties may have been significantly changed during the processes of mechanical fibrillation or chemical treatments. Simultaneously, the fraction of surface functionality changes as the size of cellulosic material decreases and the hydroxyl groups at the surface of cellulosic material is different from the hydroxyl groups inside the bulk. Moreover, the hydroxyl groups at surface of crystalline cellulose are different from the hydroxyl groups in the amorphous region of cellulose. Characterization of the surface energy of CNFs is necessary. At the same time, the drying method may further impact the surface properties of NFCs and CNCs. During drying, cellulose fibrils aggregation occurs [37,38]. The method of drying influences the size of the fibril aggregate dimensions and the reaction rate of the dried cotton cellulose [38]. After drying, different morphologies, aggregation degree, and crystalline structures of NFCs and CNCs are formed [17,39]. Therefore, the effect of drying method on the surface properties of CNFs needs to be evaluated.

The objectives of this study were to measure the surface energy of the dried CNFs, including NFCs and CNCs, and to evaluate the effect of drying method thereof. Samples of NFC and CNC were each subjected to four separate drying methods: air-drying, freeze-drying, spray-drying, and supercritical-drying. The morphologies of CNFs in suspensions and in dry form were examined using a transmission electron microscope and a scanning electron microscope. The surface energy measurements, including dispersion component of surface energy and acid and base parameters, on each dried sample were performed using inverse gas chromatography at infinite dilution (IGC-ID) and column temperatures: 30, 40, 50, 55, and 60 °C. The IGC measurement of supercritical-dried NFCs was also conducted at column temperatures of 70, 75, and 80 °C. The effect of different drying methods on the morphologies and surface energies of NFCs and CNCs was determined. Correlation between morphology and surface energy of CNFs is discussed.

2. Experimental sections

2.1. Suspension preparation and drying

The NFC suspension was a commercial product, ARBOCEL MF40-10 at 10 wt.% from J. Rettenmaier & Sohne GMBH+CO.KG, Germany. The CNC suspension at 6.5 wt.% was obtained from the Forest Products Laboratory in Madison, Wisconsin. Before drying, distilled water was added into the original suspensions and mixed using a Speed Mixer® (Flack Tek Inc., US) for 4 min at 2000 rpm to obtain final weight concentration of CNC and NFC suspensions at 0.001 and 2 wt.%.

Different drying methods were applied to the CNF suspensions at 2 wt.%, including NFC and CNC suspensions, just after mixing. Air-drying (AD) of the two different suspensions was performed in a conditioning room with relative humidity of 65 ± 5% and temperature of 20 ± 2 °C. The suspensions were allowed to settle to a constant weight in plastic containers before collection. Prior to freeze-drying (FD), CNF suspensions (about 20 ml) were frozen in vials at a temperature of −80 °C for 24 h. Frozen suspensions were then transferred to a Virtis Freezemobile 25 SL freeze dryer, which has a condenser temperature of −80 °C and a vacuum of 11 mTorr. Lyophilization was allowed to continue for 72 h. Supercritical drying (SCD) of the prepared suspension was conducted on the Tousimis Samdri PVT-3 Critical-Point dryer. Four steps were involved in this process: (1) dehydration of CNF suspension with a series of ethanol solutions (50%, 75%, 95%, and 100%) until water was

completely replaced with ethanol, (2) replacement of ethanol with liquid CO_2, (3) pressurization and heating of the liquid CO_2 and the cellulose mixture to the supercritical conditions, and (4) slow decompression of the supercritical CO_2 to atmospheric pressure. Spray-drying of the CNF suspensions was conducted using a Buchi Mini Spray Dryer B-290 laboratory spray dryer (New Castle, DE, USA). High purity nitrogen gas was used as an injected gas to form the suspension droplets. The spray-drying process is detailed in Peng et al. [17] and Peng et al. [18]. In this study, CNF suspensions were dried at an inlet temperature of 175 °C, gas flow rate of 540 l/h, pump rate of 4.5 ml/min, and drying gas flow rate of approximately 35 m^3/h. The outlet temperatures of the spray-dryer measured for the NFCs and CNCs were 100 and 93 °C. All the dried CNFs were put in plastic bags and stored in a desiccator at ambient temperature for future use.

2.2. Transmission electron microscopy (TEM)

Drops of 0.001 wt.% NFC and CNC suspensions were deposited on carbon coated electron microscope grids and negatively stained with 2 wt.% uranyl acetate. The grids were dried in air and observed with a Philips CM10 Transmission Electron Microscope operated at an acceleration voltage of 80 kV.

2.3. Scanning electron microscopy (SEM)

SEM studies on the morphologies of dried samples were carried out using an AMR 1820 (AMRay Co.) scanning electron microscope. All samples were sputter-coated with gold before the microscopic observations were obtained. SEM images were taken at an accelerating voltage of 10 kV at various magnifications.

2.4. Inverse gas chromatography (IGC) theory

The dispersion component of surface energy and acid and base parameters of the dried CNFs were measured using inverse gas chromatography (IGC). Inverse gas chromatography (IGC) is a technique to characterize dynamic sorption of gas on a solid surface. This differs from analytical gas chromatography. The column in the IGC is filled with the sample under investigation (adsorbent) and the mobile phase consisting of a probe molecule (adsorbate) with known properties is used to evaluate the surface of the adsorbent. A pulse experiment is usually conducted to determine the surface energy of materials. A controllable amount of the probe molecule is injected and then flows with the carrier gas (helium) through the adsorbent in the column. At infinite dilution, the probe molecules are injected at very low vapor pressure which indicates that the adsorption isotherm is located in the Henry's Law region. The lateral interactions among the probe molecules are negligible and the adsorption depends only on adsorbate–adsorbent interactions [21,40]. At the same time, the number of injected molecules is unable to form full monolayer coverage and primarily interacts with high surface energy sites on the surface. The surface information obtained from IGC-ID mainly indicates a material presenting the highest activity or enthalpy of adsorption [41]. When probe molecules flow inside the IGC column, equilibrium (or quasi-equilibrium) between adsorption and desorption of the probe gas on the adsorbent can be assumed to be obtained by adjusting the carrier gas flow rate [42]. After a delay, the probe molecules exit from the column and are detected by a flame ionization detector (FID) or thermal conductivity detector (TCD).

The experimental parameter measured in IGC-ID is the retention time of the probes, which can be converted to the net specific retention volume by the following relationship [40]:

$$V_N = \frac{j}{m} \cdot F \cdot (t_R - t_0) \cdot \frac{T}{273.15} \tag{1}$$

where V_N is the net specific retention volume per gram of sample (ml/g), T is the column temperature (K), m is the weight (g) of sample packed in the column, F is the flow rate (ml/min) of carrier gas, t_R is the retention time (min) of the probe and t_0 is the retention time (min) of a reference gas (usually methane), j is the James–Martin correction, which corrects the retention time for the pressure drop in the column [43]. With the known net specific retention volume of n-alkane probes, the following relationship can be applied [40,44,45]:

$$RT \cdot \ln(V_N^{alkane}) = 2N \cdot a \cdot (\gamma_S^{LW})^{1/2} \cdot (\gamma_L^{LW})^{1/2} + C \tag{2}$$

where V_N^{alkane} is the net specific retention volume of n-alkane probes on the adsorbent; γ_L^{LW} and γ_S^{LW} are the dispersion components of surface energy of the probes and the adsorbent surface; "N" is Avogadro's number; "a" is the surface area of the probe molecule; "C" is a constant, depending on the reference state of adsorption. According to the Eq. (2), plot of $RT \cdot \ln(V_N^{alkane})$ against $(a \cdot (\gamma_L^{LW})^{1/2})$ yields a straight line with the slope equals to $(2N \cdot (\gamma_S^{LW})^{1/2})$, from which the dispersion component of surface energy of adsorbent can be determined. The molecular descriptor $(a \cdot (\gamma_L^{LW})^{1/2})$ used in this plot is derived by Schultz et al. [44].

To characterize the Lewis acid–base properties of a solid surface, IGC running using extra polar probes is needed. The free energy of adsorption caused by the Lewis acid–base interactions (ΔG_A^{A-B}) can be determined by subtracting the dispersion component contribution (ΔG_A^{ref}) from the total free energy of adsorption (ΔG_A^{polar}) using the following equation:

$$\begin{aligned} -\Delta G_A^{A-B} &= -(\Delta G_A^{polar} - \Delta G_A^{ref}) \\ &= -(RT \cdot \ln(V_N^{polar}) - RT \cdot \ln(V_N^{ref})) \end{aligned} \tag{3}$$

where $RT \cdot \ln(V_N^{ref})$ in Eq. (3) is the corresponding value of $RT \cdot \ln(V_N^{alkane})$ with the molecular descriptor $(a \cdot (\gamma_L^{LW})^{1/2})$ of the polar probe. With the polar probes running at several different column temperatures, a plot of ΔG_A^{A-B} with the Kelvin temperature (T) generates a straight line with the y-intercept as the enthalpy of adsorption related to acid–base interaction (ΔH_A^{A-B}). The acid and base parameters are then can be calculated using the following equation [46–49]:

$$-\frac{\Delta H_A^{A-B}}{AN^*} = K_A\left(\frac{DN}{AN^*}\right) + K_D \tag{4}$$

where AN^* and DN are the acceptor number and donor number of the probes [46,47]; K_A and K_D are acid and base parameters of the adsorbent, which can be determined by plotting $-\Delta H_A^{A-B} AN^*$ against (DN/AN^*). The linear slope and y-intercept are K_A and K_D, respectively. These numbers are dimensionless and provide comparative information about the material surface under investigation.

2.5. Surface property determinations

Air-dried CNF bulk materials (NFCs and CNCs) were ground into fines using a mortar and pestle. All the other dried CNFs were tested directly after drying. The IGC experiments were conducted on a SMS-iGC (Surface Measurement Systems, London, UK). The testing columns were prepared by filling the dried CNFs into a pre-silanized glass tube 30 cm in length and 4 mm in inner diameter using an electric vibrator. The ends of the glass tube were plugged with silanized glass wool. The sample weights packed in the column differed for various CNFs, ranging from 0.02 to 1.5 g. Helium was used as the carrier gas, and methane was employed as a reference probe. The analytical grade probes from Sigma–Aldrich Ltd. (St. Louis, US)

Table 1
Physical constants for probes used in IGC experiments.[a]

Probe	Surface tension (γ_L^{LW}, mJ/m^2)	Cross sectional area (a, m^2)	DN[b] (kcal/mol)	AN*[c] (kcal/mol)
n-Hexane	18.4	5.15E−19	–	–
n-Heptane	20.3	5.73E−19	–	–
n-Octane	21.3	6.3E−19	–	–
n-Nonane	22.7	6.9E−19	–	–
n-Decane	23.4	7.5E−19	–	–
Ethyl acetate (EA)	19.6	3.3E−19	17.1	1.5
Tetrahydrofuran (THF)	22.5	2.9E−19	20	0.5
Acetone	16.5	3.4E−19	17.0	2.5
Chloroform	25	4.4E−19	0	5.4

[a] Data from literature [46,50,51].
[b] DN = donor number.
[c] AN* = acceptor number.

used in this study and their physical constants are shown in Table 1. The values shown in Table 1 were extracted from the literature [46,50,51]. The retention times of probe molecules and methane were determined using an FID. All samples were measured under the same conditions of relative humidity (RH) of 0% and carrier gas flow rate of 10 standard cubic centimeters per minute (sccm) at column temperatures of 30, 40, 50, 55, and 60 °C. The evaluation of supercritical-dried NFCs was performed at temperatures of 70, 75, and 80 °C using the same procedures. The details are discussed in the next section. Prior to the experiments, the columns were conditioned *in situ* for 4 h at a temperature of 30 °C, RH of 0%, and carrier gas flow rate of 10 sccm. The vapor concentration of the probe molecules injected into the system was 0.03 p/p_0 (p is the partial pressure, p_0 is the vapor pressure). Retention time for all the probes at different temperatures was determined by the peak maximum method [40]. The dispersion component of surface energy is then calculated according to the method of Schultz et al. [44]. The acid–base characteristics of the cellulose materials are evaluated based on the theories of Gutmann [46], Schultz and Lavielle [49], and Fowkes [51]. Each IGC test for all the cellulose samples was performed in duplicate.

3. Results and discussion

3.1. Morphology of CNFs in suspension and in dry form

The morphologies of NFCs and CNCs in suspensions were examined directly using a transmission electron microscope and the obtained micrographs of NFCs and CNCs are shown in Fig. 1. Both NFC and CNC showed needlelike fibrils. NFCs showed greater dimensions (diameter and length) than those of CNCs. The diameter of individual NFC is around 10 nm with length ranging from about 100 nm to several hundred nanometers. A portion of relatively short and large cell wall sections (chunks) in the NFC suspension which was generated during the mechanical fibrillation process were also observed (Fig. 1a). The diameter of the large cell wall section shown in Fig. 1a is around 250 nm. When compared to NFCs, CNCs showed more uniform distributed particles, which is the expectation of manufacturing CNFs using a chemical process. The diameters are below 10 nm and the lengths are in the range of tens of nanometers to several hundred nanometers. It is worth noting that entanglement of NFC and CNC fibrils occurred when air dried at a concentration of 0.001 wt.%. Simultaneously, NFCs tend to form significantly more network connections among individual fibrils than those of CNCs as shown in Figs. 1.

Morphologies of the air-dried NFCs and CNCs are shown in Fig. 2a and b. The two suspensions formed solidly packed bulk materials with different surface morphologies. The water evaporation process was detailed in Peng et al. [17]. Agglomeration of different sizes of NFCs was observed on the surface of air-dried NFC. Parts of the NFCs were short in length and large in diameter (Fig. 2a) which is consistent with the observations in Fig. 1a and b. The surfaces of dried CNCs were much smoother than those of NFCs, indicating an even denser packing of CNCs than for NFCs. This is attributed to the much smaller size of CNCs in the suspensions compared to that of NFCs. The morphologies of freeze-dried NFCs and CNCs are shown in Fig. 2c–f. The dried samples from the two suspensions formed similar ribbon-like (or platelet) materials with different sizes, differing from air-dried CNFs. The large length (several hundred nanometers) and width (tens to hundreds of micrometers) are the result of the lateral agglomeration of CNFs. This lateral fibril aggregation was discussed in detail in Peng et al. [17]. The thickness of these ribbon-like materials can reach nanometer scale. A close-up evaluation of the surface morphologies shows that the freeze-dried NFCs (Fig. 2d and f) are similar to those that were air dried (Fig. 2a and b). The surface of freeze-dried CNCs (Fig. 2f) is smoother than that of air-dried CNCs (Fig. 2b). During the freeze drying process, the nanofibrils were first confined in the space between ice crystals during the freezing process [52], increasing the concentration of nanofibrils locally. At this point, the interaction among cellulose nanofibrils is enhanced and the nanofibrils form a similar agglomerate structure as occurring in the case of the air-drying process. Therefore, the surface morphology of freeze-dried NFCs is similar with air-dried NFCs. However, the flow of water vapor from inside of the bulk materials (slow evaporation of water) during the air-drying process may disturb the surface morphology of CNC because of its denser packing. This is not the case for the freeze-dried CNC. No inside water evaporation occurred in the freeze-dried CNCs, forming a much smoother surface (Fig. 2f) than that of the air-dried CNCs (Fig. 2b).

The morphologies of spray-dried NFCs and CNCs are shown in Fig. 3a and b. NFCs and CNCs with a size distribution ranging from nanometer to several microns were obtained. Fibrous NFCs were formed by attaching small NFC fibrils to longer NFC fibrils during the spray-drying process. Irregular agglomerates of NFCs were also obtained. Spray-drying CNCs produced spherical and mushroom cap (or donut) shaped particles. The detailed information related to spray-drying is reported in previous papers [17,18]. The morphologies of supercritical-dried NFCs are shown in Fig. 3c and d. During the process of supercritical-drying, agglomeration of CNFs was minimized because of the zero surface energy of supercritical carbon dioxide [17,53,54]. Drying of CNC suspension using supercritical-drying process was not successful [17]. As seen in the SEM micrographs of Fig. 3c and d, nano-scale NFCs with diameters of about 100–200 nm were observed. These micrographs have also demonstrated the large diameter and short length fibrils which exist in the NFC suspension. Simultaneously, highly entangled networks of fine NFC individual fibrils were observed in the SEM micrographs (Fig. 3c and d). When compared to the other drying methods (air-drying, freeze-drying, and spray-drying), supercritical-drying preserved the original NFC nature to the upmost extent in surface morphologies, including size and shape.

3.2. Dispersion component of surface energy of the dried CNFs

The adsorption behavior of *n*-alkane probes on the dried CNFs is determined by the dispersion component of surface energy. Using the obtained net specific retention volume of the *n*-alkane probes, the dispersion component of surface energy of the CNFs is obtained using Eq. (2). A typical plot of $RT \ln V_N^{alkane}$ against the molecular descriptor $(a(\gamma_L^{LW})^{1/2})$ is shown in Fig. 4. The dispersion components of surface energy as a function of temperature are shown in Tables 2 and 3. For the various dried CNFs, different sample

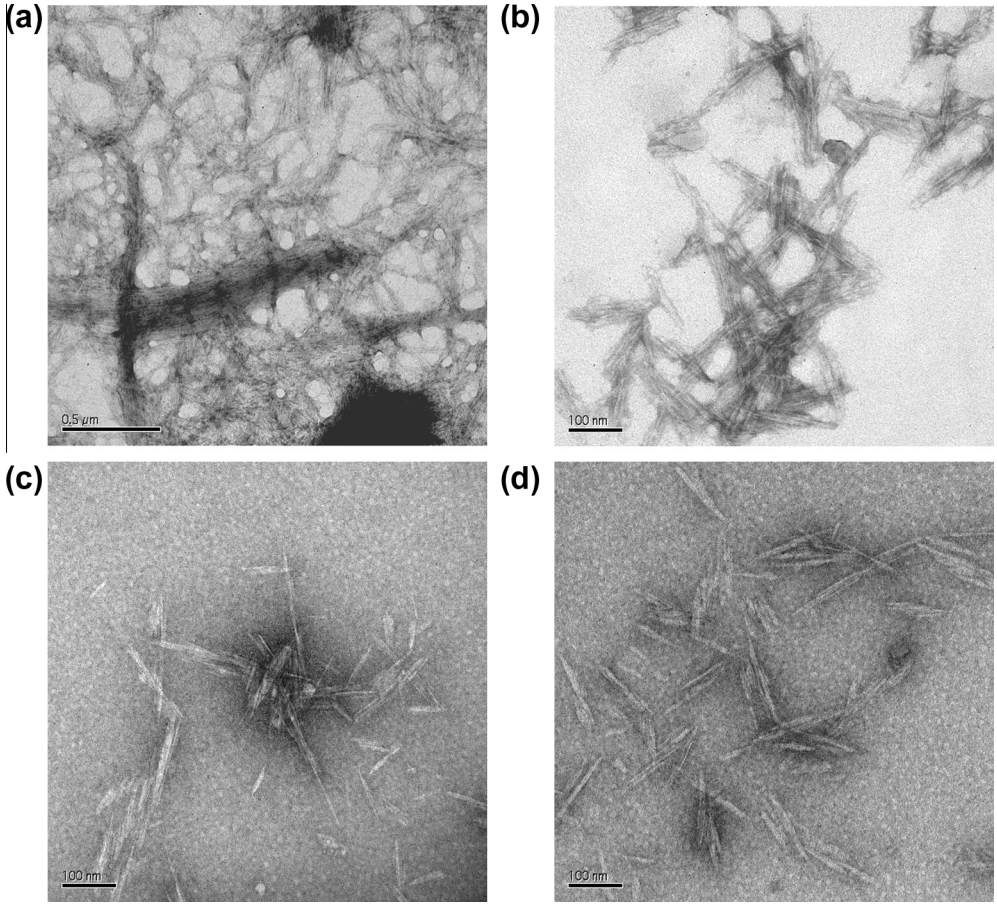

Fig. 1. TEM micrographs of NFCs (a and b) and CNCs (c and d).

masses were needed to conduct the IGC experiments because of their different morphologies (Figs. 2 and 3) and structures [19].

Calculation of the dispersion component of surface energy generally requires the retention time of four (or above) *n*-alkane probes. During the IGC experiments on the supercritical-dried NFCs, only the retention times of two probes (*n*-hexane and *n*-heptane) were obtained at 30, 40, and 50 °C and three probes (*n*-hexane, *n*-heptane, and *n*-octane) were obtained at 55 and 60 °C. It was hypothesized that the peaks for the other *n*-alkane probes took too long to elute at these measurement temperatures (over 60 min which is maximum value provided by the equipment) because they were not observed in the chromatograms of the IGC runs. Under this circumstance, the dispersion components of surface energy of the supercritical-dried NFC obtained using only two or three probes were highly variable and were deemed not reliable. Therefore, the dispersion component of surface energy of the supercritical-dried NFCs at 30, 40, 50, 55, and 60 °C are not shown in Table 2. Measurement of the surface energies of the supercritical-dried NFCs were performed at higher temperatures of 70, 75, and 80 °C using the same two columns tested from 30 to 60 °C. The results are shown in Table 3. The dispersion components of surface energy for the supercritical-dried NFCs are 60.5 ± 0.4, 54.9 ± 0.9, and 51 ± 1.1 mJ/m^2 at 70, 75, and 80 °C. The dispersion components of surface energy of supercritical-dried NFCs decreased linearly with increasing temperature. The temperature coefficients of dispersion component of surface energy ($d\gamma^{LW}/dT$) are −0.81 and −1.09 mJ m^{-2} K^{-1} and the linear correlation coefficients (R^2) are 0.99 and 0.98 as shown in Table 3. Based on the linear relationship between the dispersion component of surface energy and column temperature, the dispersion component of surface energy of supercritical-dried NFCs at 30, 40, 50, 55, and 60 °C can be obtained by extrapolation. At 30, 40, 50, 55 and 60 °C, the dispersion component of surface energy of supercritical-dried NFCs are 98.3 ± 5.75, 88.8 ± 4.4, 79.3 ± 3.0, 74.5 ± 2.3 and 69.7 ± 1.6 mJ/m^2, which are shown in Table 3.

A comparison of the dispersion components of surface energy for the dried CNFs at temperatures of 30, 40, 50, 55, and 60 °C is shown in Table 2 and Fig. 5. Different drying methods resulted in different dispersion component of surface energy of the dried CNFs. Supercritical-dried NFCs have the highest dispersion component of surface energy when compared to CNFs dried by other methods. Supercritical-drying formed single NFCs as shown in Fig. 3c and d. Supercritical-drying preserved the nature of NFCs with the lowest crystallinity index [19]. A higher dispersion component of surface energy of cellulose (116 mJ/m^2) at 30 °C generated by solvent exchange was reported by Lee and Luner [22]. During the supercritical-drying process, the organic solvent ethanol was also used to replace the water in the NFC suspension. After drying, reduced agglomeration of NFCs was observed with presumably more exposed surface hydroxyl groups than those of CNFs dried by other methods. The supercritical-dried NFCs have the lowest moisture content of the dried NFCs shown via thermogravimetric analysis [19]. Therefore, more hydroxyl groups which mainly contribute to the dispersion component of surface energy of cellulose materials [25] are exposed on the surface, resulting in the high dispersion component of surface energy. Simultaneously, the highest temperature coefficient of dispersion component of surface energy (−0.95 ± 0.14 mJ/(m^2 K)) is obtained for the supercritical-dried NFCs (Table 3) within the temperature range of 70–80 °C, followed by the air-dried CNCs (−0.60 mJ/(m^2 K)) within the

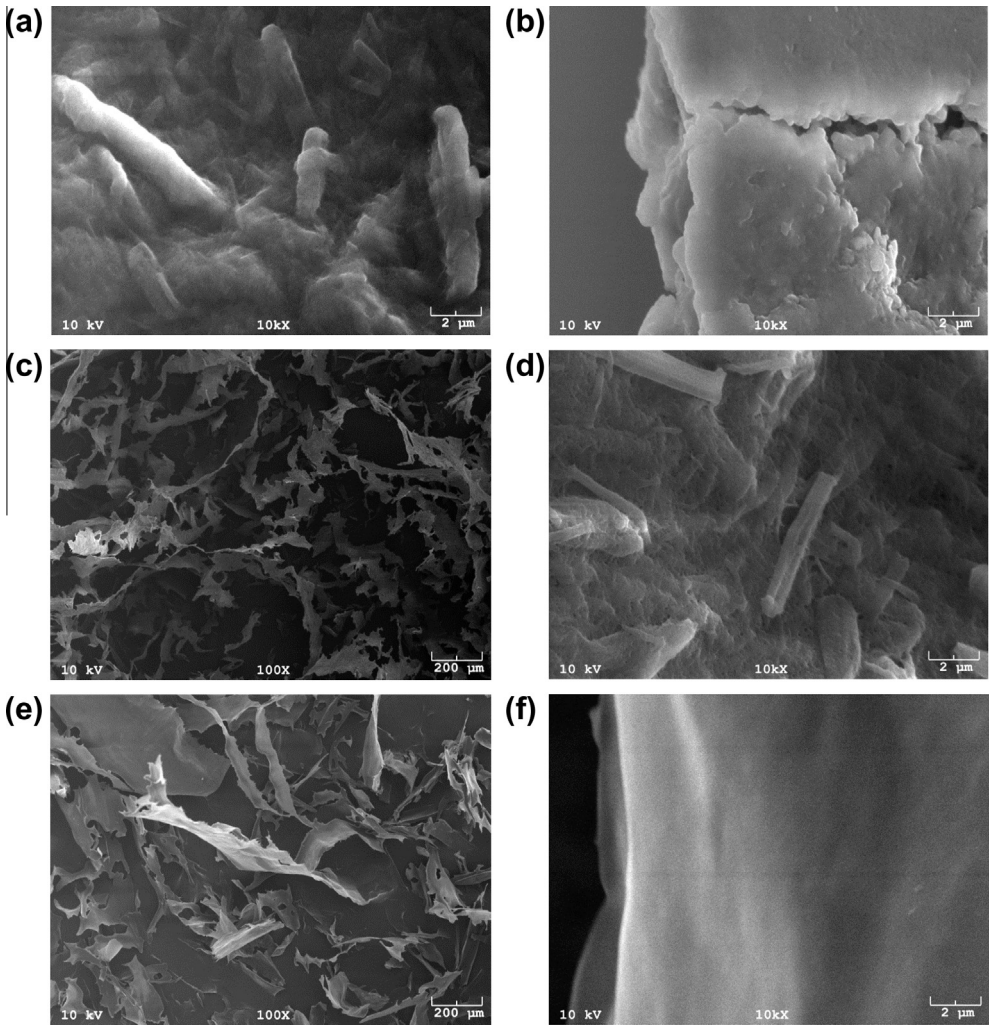

Fig. 2. SEM micrographs of the dried CNFs: (a) air-dried NFCs, (b) air-dried CNCs, (c) and (d) freeze-dried NFCs, and (e) and (f) freeze-dried CNCs.

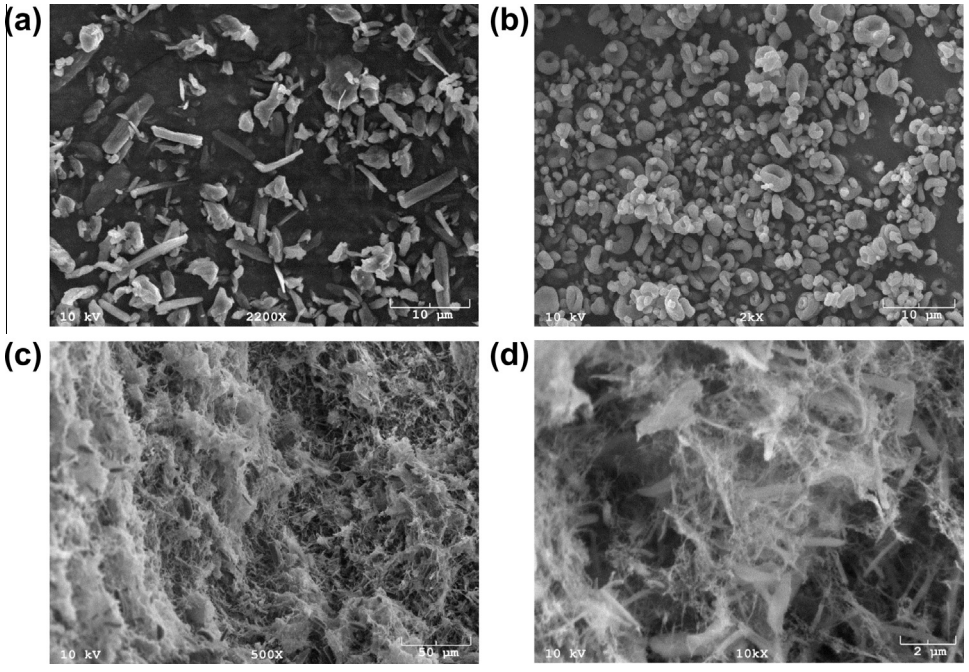

Fig. 3. SEM micrographs of the dried CNFs: (a) and (b) supercritical-dried NFCs, (c) spray-dried NFCs, and (d) spray-dried CNCs.

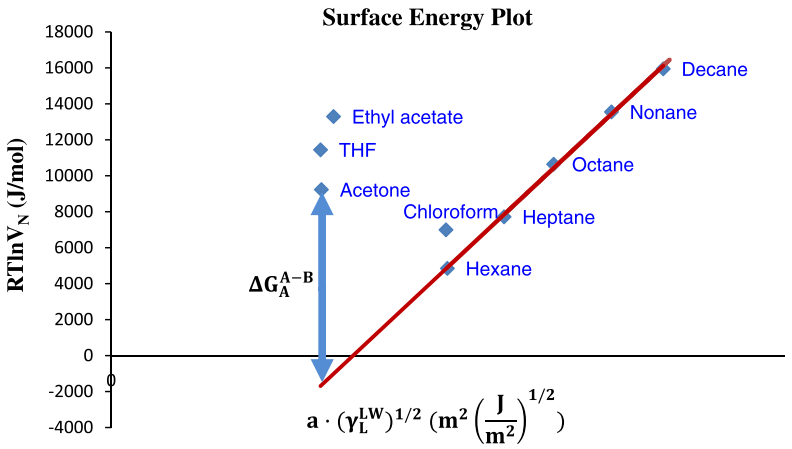

Fig. 4. Schematic calculation process for surface energy.

Table 2
The dispersion component of surface energy of the dried CNFs.

Sample	Drying method	No.	Dispersion component of surface energy (γ_S^{LW}, mJ/m^2)						$d\gamma_L^{LW}/dT$ (mJ/(m^2 K))	R^2
			Mass (g)	30 °C	40 °C	50 °C	55 °C	60 °C		
NFC	AD[a]	1	0.953	52.0	50.3	47.9	46.3	44.4	−0.25	0.98
		2	0.964	52.8	50.9	49.1	47.0	45.0	−0.27	0.95
	FD[a]	1	0.201	43.1	42.9	39.8	38.5	38.6	−0.18	0.90
		2	0.245	45.5	43.6	41.8	39.7	39.6	−0.21	0.98
	SD[a]	1	0.363	53.7	50.9	48.2	46.3	44.8	−0.29	1.00
		2	0.257	51.5	49.5	46.9	45.7	43.1	−0.27	0.97
	SCD[a]	1	0.039	–	–	–	–	–	–	–
		2	0.024	–	–	–	–	–	–	–
CNC	AD[a]	1	1.228	68.5	61.4	55.6	53.2	50.2	−0.60	1.00
		2	1.057	65.3	60.2	53.4	50.6	47.3	−0.61	1.00
	FD[a]	1	0.228	45.6	42.0	40.5	35.8	35.6	−0.34	0.94
		2	0.227	47.3	42.2	41.4	38.0	38.9	−0.28	0.89
	SD[a]	1	0.259	59.7	58.2	55.5	53.2	51.3	−0.28	0.96
		2	0.315	61.2	59.1	55.2	53.8	53.3	−0.28	0.98

[a] AD = air-drying, FD = freeze-drying, SD = spray-drying, SCD = supercritical-drying.

Table 3
The surface energy of supercritical-dried NFCs.

Sample	Mass (g)	Dispersion component of surface energy γ_S^{LW}, mJ/m^2)								$d\gamma_S^{LW}/dT$ (mJ/(m^2 K))	R^2
		30 (°C)	40 (°C)	50 (°C)	55 (°C)	60 (°C)	70 (°C)	75 (°C)	80 (°C)		
SCD[a] NFC	0.039	92.5	84.4	76.3	72.2	68.1	60.1	55.7	52.1	−0.81	0.99
	0.024	104.0	93.1	82.2	76.8	71.3	60.8	54.0	49.9	−1.09	0.98

[a] SCD = supercritical-dried.

temperature range of 30–60 °C (Table 2). All the dispersion components of surface energy decreased linearly with increasing temperature. The temperature coefficients of dispersion component of surface energy ($d\gamma^{LW}/dT$) and the linear correlation coefficient (R^2) for all the other CNF samples are shown in Tables 2. All the other dried CNFs have much smaller temperature coefficients than the supercritical-dried NFCs and air-dried CNCs, ranging from −0.18 to −0.34 mJ/(m^2 K) (Table 2). These values (−0.18 to −0.34 mJ/(m^2 K)) are comparable with the temperature coefficient data reported by other investigators [24,30]. The high temperature coefficient values of supercritical-dried NFCs (−0.95 mJ/(m^2 K)) and air-dried CNCs (−0.60 mJ/(m^2 K)) indicate a much more significant effect of temperature on the dispersion component of surface energies of supercritical-dried NFCs and air-dried CNCs compared to the CNFs dried by other methods. At higher IGC measurement temperatures, the thermal energy drives greater propensity for the reorientation of the surface hydroxyl groups for supercritical-dried individual NFC. In the glassy state of cellulose fibers, localized, thermally activated motions are able to force molecules in amorphous regions to rearrange [55,56]. Under this circumstance, hydrogen bonds built among the cellulose chains change with increasing temperature, forming more inter-chain hydrogen bonds and more stable sheet structures [57]. The dispersion component of surface energy of cellulosic materials was observed to depend mostly on the presence and concentration of free hydroxyl groups on the surface [25]. Therefore, the effect of temperature on the

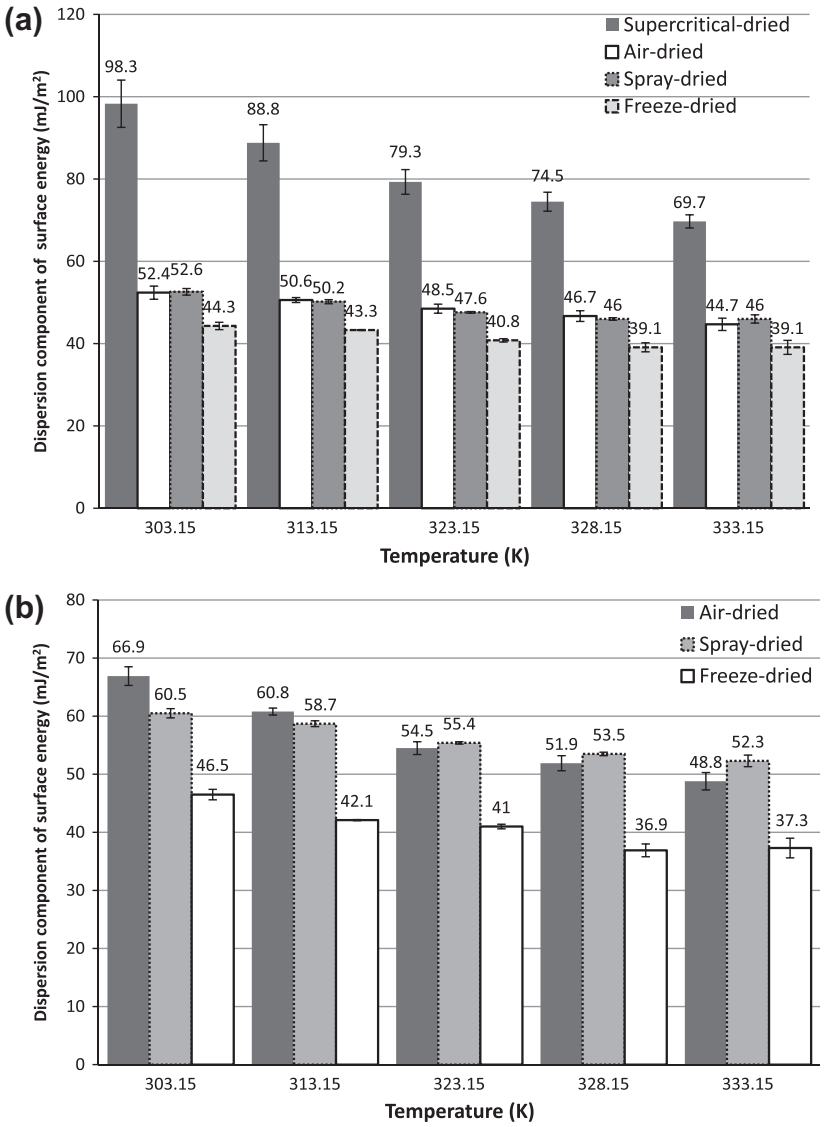

Fig. 5. Comparison of the dispersion component of surface energies of CNFs dried with different methods: (a) NFCs and (b) CNCs.

dispersion component of surface energy of supercritical-dried NFCs becomes more significant than for the other aggregated CNFs. This phenomenon may partially explain that the reliable surface energy data can be obtained at higher measurement temperatures of 70, 75, and 80 °C compared to that at the lower temperatures (30–60 °C). The rearrangement of the hydroxyl groups forming inter-hydrogen bonds among cellulose fibrils at higher temperatures (70, 75, and 80 °C) eliminates the strong attraction of probes through van der Waals force in the IGC columns because of the greater number of free hydroxyl groups on the surface of supercritical-dried NFCs.

For the IGC measurement of the dried NFCs under the same temperature, air-drying and spray-drying formed materials that possessed a similar dispersion component of surface energies. The dispersion components of surface energy for air-dried NFCs at 30, 40, 50, 55, and 60 °C are 52.4 ± 0.4, 50.6 ± 0.3, 48.5 ± 0.6, 46.6 ± 0.4, and 44.7 ± 0.3 mJ/m^2 while these values for spray-dried NFCs are 52.6 ± 1.1, 50.2 ± 0.7, 47.6 ± 0.7, 46 ± 0.6 and 44 ± 0.9 mJ/m^2. Air-drying of NFC suspensions was performed at room temperature for several days. The slow drying rate in this process allowed the proper orientation of the nanofibrils with the establishment of a hydrogen-bonding network, forming bulk materials (Fig. 2a). The interactions among nanofibrils through hydrogen bonding may approach a maximum during the nanofibril position rearrangement. For spray-drying, the water evaporation rate is higher than that for air-drying. Increased water evaporation is driven by the relatively higher temperature of spray-drying process (100 °C). When compared to air-drying, the higher drying rate of spray-drying may limit the rearrangement of cellulose nanofibrils. Therefore, the spray-dried NFCs were assumed to form fewer hydrogen bonds, indicating more exposed hydroxyl groups and higher dispersion component of surface energy than that of air-dried NFCs. However, the possibility of forming denser packing of NFCs at the drying temperature of 100 °C would lower the dispersion component of surface energy of spray-dried NFCs compared to those of air-dried NFCs. The denser packing of spray-dried NFCs can be demonstrated by decreased water accessibility, i.e. the less final moisture content (2.8 wt.%) of spray-dried NFCs than that of air-dried NFCs (4.1 wt.%) [19]. As a result, the dispersion component of surface energy of spray-dried and air-dried NFCs were similar. This was determined by the compounding effects of different NFC rearrangement and drying temperature in air-drying and spray-drying processes.

The dried CNCs were different. Air-dried CNC exhibited a higher dispersion component of surface energy than the spray-dried CNC at 30 and 40 °C. The dispersion component of surface energy for

air-dried CNC at 30 and 40 °C are 66.9 ± 1.6, 60.8 ± 0.6 mJ/m^2 while the values for spray-dried CNC are 60.5 ± 0.8 and 58.7 ± 0.5 mJ/m^2. CNC is much stiffer than NFC because of the digestion of the amorphous regions in the manufacturing process of CNC. During the air-drying process, the effect of CNC rearrangement on the dispersion component of surface energy is not as significant as that for the air-dried NFCs. When compared to spray-drying, the smaller size of CNCs formed less aggregated agglomerates during the process of air-drying. Evaporation of inside water in the bulk materials may disturb the connections among CNCs which can be shown by the rough surface in Fig. 2b. Compared to the spray-dried CNCs, the higher dispersion component of surface energy of air-dried CNCs may be partially caused by the greater number of exposed hydroxyl groups on the surface. At the same time, spray-drying appears to promote the formation of inter-molecular hydrogen bonds by dehydration among CNCs at this relatively high temperature (93 °C) [57]. The formation of inter-molecular hydrogen bond would result in a relatively lower dispersion component of surface energy of spray-dried CNCs than that of air-dried CNC surface. The assumption of the temperature effect can be validated by the much higher temperature coefficients of dispersion component of surface energy during the measurement for air-dried CNCs (0.60 mJ/(m^2 K)) than those of spray-dried CNCs (0.28) and air-dried NFCs (0.26 mJ/(m^2 K)). The less aggregated CNCs have greater freedom and propensity to rearrange their surface hydroxyl groups under the effect of thermal treatments, resulting in higher temperature coefficients of the dispersion component of surface energy. Similarly, higher drying temperature during the spray-drying process depressed the dispersion component of surface energy of spray-dried CNCs compared with air-dried CNCs. The hypothesis of the effect of temperature on dispersion component of surface energy is further validated by the effect of rising IGC column temperature. At the IGC column temperatures of 50, 55, and 60 °C, the dispersion component of surface energy of air-dried CNCs are 54.5 ± 1.1, 51.9 ± 1.3, and 48.8 ± 1.5 mJ/m^2 while the values for spray-dried CNCs are 55.4 ± 0.2, 53.5 ± 0.3 and 52.3 ± 1.0 mJ/m^2. The differences of the dispersion component of surface energy between air-dried and spray-dried CNCs decreased from 6.4, 2.1, −0.9, −1.6, and −3.5 mJ/m^2 as the IGC measurement temperature increased from 30, 40, 50, 55, to 60 °C (Table 2 and Fig. 5). At the IGC measurement temperatures above 50 °C, the dispersion component of surface energy of spray-dried CNCs is greater than that of air-dried CNCs. The effect of temperature (IGC column temperature or drying temperature) mainly dominates the dispersion component of surface energy of the dried CNCs. Simultaneously, spray-dried NFCs and CNCs showed practically identical temperature coefficients (0.28 mJ/(m^2 K)) of the dispersion component of surface energy. The spray-drying process diminished the effect of temperature on the dispersion component of surface energy of the obtained CNFs. The rearrangement of surface hydroxyl groups and temperature experience of the cellulose fibers during the spray-drying process is the main reason for this observation.

A slightly higher dispersion component of surface energy of air-dried and spray-dried CNCs was observed when compared to the air-dried and spray-dried NFCs, respectively. However, freeze-drying produced NFCs and CNCs both with similar dispersion components of surface energy and all the dispersion components of surface energy are lower than those of air-dried and spray-dried samples (Fig. 2). The dispersion component of surface energy of the freeze-dried NFCs at 30, 40, 50, 55, and 60 °C are 44.3 ± 1.2, 43.3 ± 0.4, 40.8 ± 1.0, 39.1 ± 0.6, and 39.1 ± 0.5 mJ/m^2. The dispersion components of surface energy for the freeze-dried CNCs are similar: 46.5 ± 0.9, 42.1 ± 0.1, 41.0 ± 0.5, 36.9 ± 1.1, and 37.3 ± 1.7 mJ/m^2. Identical drying methods generated similar surface energies on different materials, indicating the process of freeze-drying is the dominating factor which impacts the surface properties of the CNFs. The freeze-drying process consists of three stages: pre-freezing, primary drying and secondary drying. In the pre-freezing stage, the cellulose nanofibrils were separated from water as water changes to ice crystals, thus creating more concentrated areas of cellulose nanofibrils. Within the sample, high concentrations of nanofibrils enhance the interaction among the nanofibrils and form different degrees of cellulose agglomerates. Agglomeration of cellulose nanofibrils blocked the hydroxyl groups on each nanofibril surface and decreased their exposure density. As a result, the dispersion component of surface energy decreases. As freeze-drying proceeds, the bound water left from the primary drying stage is desorbed from the cellulose nanofibrils and further agglomeration of cellulose nanofibrils continues. Therefore, freeze-drying decreased the dispersion component of surface energy of the dried NFC and CNC more significantly than the other drying methods. In the case of CNCs, a smoother surface was generated during the freeze-drying (Fig. 2f) compared to air-drying and spray-drying, validating that the denser packing of CNCs caused the lower dispersion component of surface energy. Another reason is the low temperature treatment on the cellulose nanofibrils. A study was conducted to investigate the effect of pre-freezing as a pre-treatment on the surface properties of wood [58]. Their results indicated that pre-freezing treated wood produces a lower surface energy than unfrozen samples.

3.3. Acid and base parameters of the dried CNFs

With additional IGC measurements using polar probes, the Lewis acid–base characteristics of the dried CNFs can be determined in the IGC-ID experiments. Four polar probes were used in this study: ethyl acetate (EA), tetrahydrofuran (THF), acetone, and chloroform. Among the four chemicals, THF is considered a monopolar basic probe, chloroform is a monopolar acidic probe, and the other two are amphoteric probes (Table 1). Based on the theory of Schultz et al. [44], no specific interaction occurs between two acids or two bases. The free energy of adsorption for the polar probes caused by acid–base interaction (Δ_A^{A-B}) is calculated using Eq. (3) and the acid–base components of surface energy are determined using Eq. (4) over several temperature measurements. The acid and base parameters calculated for all the dried CNFs are shown in Table 4. The acid and base parameters indicates that the dried CNFs were amphoteric (acidic and basic) with dominant basic characteristic ($K_B > K_A$). The acid and base parameters for

Table 4
The acid and base parameters of the dried CNFs.

Sample	Drying method	No.	Acid and base parameters			
			Mass (g)	K_A	K_B	R^2
NFC	AD[a]	1	0.953	0.37	0.67	0.98
		2	0.964	0.37	0.63	0.98
	FD[a]	1	0.201	0.40	0.64	0.97
		2	0.245	0.34	0.51	0.98
	SD[a]	1	0.363	0.45	0.69	0.98
		2	0.257	0.38	0.57	0.98
	SCD[a]	1	0.039	0.61	1.14	0.99
		2	0.024	0.76	1.42	0.98
CNC	AD	1	1.228	0.46	0.81	0.98
		2	1.057	0.44	1.01	0.98
	FD	1	0.228	0.37	0.61	0.98
		2	0.227	0.36	0.77	0.97
	SD	1	0.259	0.66	1.37	0.98
		2	0.315	0.66	1.41	0.99

[a] AD = air-drying, FD = freeze-drying, SD = spray-drying, SCD = supercritical-drying.

supercritical-dried NFCs are calculated based on the IGC measurements at 70, 75, and 80 °C and the values are 0.69 ± 0.08 and 1.28 ± 0.14 (Table 4). When compared to NFCs dried by other three methods (air-drying, freeze-drying, and spray-drying), supercritical-drying produced NFCs with higher acid and base numbers. However, no significant difference was observed on the ratios of base to acid numbers for all the dried NFCs, ranging from 1.5 to 1.9. At the same time, no obvious difference was observed among the acid and base numbers of the NFCs produced from air-drying, freeze-drying, and spray-drying. The CNC samples show slightly higher basic numbers (K_B) than the NFCs dried using the same methods. The ratios of base number to acid number for the CNCs are also slightly higher than those of the NFCs. Grafting of the sulfate group (strong donor group) to the outer surface of cellulose nanocrystals changes the nature of the CNC surface [59,60].

4. Conclusions

The effect of four drying methods on the surface properties of CNFs, including NFCs and CNCs, were investigated by scanning electron microscopy and inverse gas chromatography at infinite dilution (IGC-ID): air-drying, freeze-drying, spray-drying, and supercritical-drying. The surface energy measurements, including dispersion component of surface energy and acid and base parameters, were conducted at the temperatures of 30, 40, 50, 55, and 60 °C. The surface energy measurement of supercritical-dried NFCs was also conducted at column temperatures of 70, 75, and 80 °C. Each drying method produced unique CNFs with different surface morphologies and surface energies. Supercritical-drying produced entangled individual NFCs with the highest dispersion component of surface energy of 98.3 ± 5.75, 88.8 ± 4.4, 79.3 ± 3.0, 74.5 ± 2.3 and 69.7 ± 1.6 mJ/m^2 at 30, 40, 50, 55 and 60 °C. Higher temperature measurement of the dispersion component of surface energy for supercritical-dried NFCs at 70, 75, and 80 °C decreased the values to 60.5, 54.9, and 51 mJ/m^2. Different degrees of agglomeration were observed for CNFs produced by air-drying, freeze-drying, and spray-drying, influencing the surface energies. The dispersion component of surface energy of the freeze-dried NFCs (44.3 ± 0.4 mJ/m^2 at 30 °C) and CNCs (46.5 ± 0.9 mJ/m^2 at 30 °C) were the lowest among all the CNFs. Pre-freezing treatment mainly contributes to the observed differences in surface energy. The dispersion component of surface energy of all the dried CNFs decreased linearly with increasing temperatures from 30 to 60 °C. This is also true for supercritical-dried NFCs from 70 to 80 °C. The temperature coefficients of the dispersion component of surface energy ($d\gamma^{LW}/dT$) for supercritical-dried NFCs from 70 to 80 °C (−0.95 ± 0.14 mJ/(m^2 K)) and air-dried CNCs from 30 to 60 °C (0.61 ± 0.01 mJ/(m^2 K)) were much greater than for the other drying treatments, indicating a significant effect of temperature on dispersion component of surface energy.

The acid–base components obtained from the IGC measurements indicated that the dried CNFs were amphoteric (acidic and basic) although predominantly basic in nature. The CNC samples show slightly higher basic numbers (K_B) than the NFCs using the same drying methods. The ratios of base number to acid number for the CNCs are also slightly higher than those of the NFCs. Grafting of the sulfate group (strong donor group) to the CNCs outer surface is probably the reason causing the different acid and base parameters of CNCs and NFCs.

Acknowledgments

We acknowledge the finical support from Maine Economic Improvement Fund and the USDA Forest Service Forest Product Laboratory Project Number 11-JV-11111124-079. The content and information does not necessarily reflect the position of the funding agencies. Much appreciation goes to J. Rettenmaier & Söhne GMBH Company for donating the nanofibrillated cellulose.

References

[1] D. Klemm, B. Philipp, T. Heinze, U. Heinze, W. Wagenknecht, Comprehensive Cellulose Chemistry, Fundamentals and Analytical Methods, vol. 1, Wiley-VCH, New York, USA, 1998.
[2] R.J. Moon, A. Marini, J. Nairn, J. Simonsen, J. Youngblood, Chem. Soc. Rev. 40 (2011) 3941–3994.
[3] R. Kolakovic, L. Peltonen, T. Laaksnen, K. Putkisto, A. Laukkanen, J. Hirvonen, AAPS PharmSciTech 12 (2011) 1366–1373.
[4] A. Dufresne, Nanocellulose: From Nature to High Performance Tailored Materials, Walter de Gruyter, Berlin, Germany, 2012.
[5] D. Fengel, G. Wegener, Wood: Chemistry, Ultrastructure, Reactions, De Gruyter, Berlin, Germany, 1998.
[6] A. Chakraborty, M. Sain, M. Kortschot, Cellulose microfibres as reinforcing agents for structural materials. In: K. Oksman, M. Sain (Eds.), Cellulose Nanocomposites: Processing, Characterization and Properties. American Chemical Society, Washington, DC, 2005, pp. 169–186.
[7] D.J. Gardner, G.S. Oporto, R. Mills, M.A.S.A. Samir, J. Adhes. Sci. Technol. 22 (2008) 545–567.
[8] F.W. Herrick, R.L. Casebier, J.K. Hamilton, K.R. Sandberg, J. Appl. Polym. Sci.: Appl. Polym. Symp. 37 (1983) 797–813.
[9] M.A. Hubbe, O.J. Rojas, L.A. Lucia, M. Sain, BioResources 3 (2008) 929–980.
[10] T. Saito, Y. Nishiyama, J. Putaux, M. Vignon, A. Isogai, Biomacromolecules 7 (2006) 1687–1691.
[11] J. Bloch, UMaine to Build Nation's Only Cellulose Nanofibrils Pilot Plant, 2011. <http://umaine.edu/news/blog/2011/10/28/umaine-to-build-nation's-only-cellulose-nanofibrils-pilot-plant/>.
[12] W. Ferguson, New Scientist 2878 (2012) 24.
[13] R. Wallace, USDA under Secretary Sherman Unveils Nanocellulose Production Facility, 2012. <http://blogs.usda.gov/2012/08/03/usda-under-secretary-sherman-unveils-nanocellulose-production-facility/>.
[14] I. Siro, D. Plackett, Cellulose 17 (2010) 459–494.
[15] D. Klemm, F. Kramer, S. Moritz, T. Lindstrom, M. Ankerfors, D. Gray, A. Dorris, Angew. Chem. Int. Ed. 50 (2011) 5438–5466.
[16] R. Kolakovic, Nanofibrillar Cellulose in Drug Delivery, University of Helsinki, Finland, Dissertation, 2013.
[17] Y. Peng, D.J. Gardner, Y. Han, Cellulose 19 (2012) 91–102.
[18] Y. Peng, Y. Han, D.J. Gardner, Wood Fiber Sci. 44 (2012) 448–461.
[19] Y. Peng, D.J. Gardner, Y. Han, A. Kiziltas, Z. Cai, M.A. Tshabalala, Influence of drying method on the material properties of cellulose nanofibrils I: thermostability and crystallinity, Cellulose (2013). Accepted for publication.
[20] D.F. Steele, R.C. Moreton, J.N. Staniforth, P.M. Youn, M.J. Tobyn, S. Edge, AAPS J. 10 (2008) 494–502.
[21] G.M. Dorris, D.G. Gray, J. Colloid Interface Sci. 77 (1980) 353–362.
[22] H.L. Lee, P. Luner, J. Wood Chem. Technol. 13 (1993) 127–144.
[23] P.N. Jacob, J.C. Berg, Langmuir 10 (1994) 3086–3093.
[24] G. Garnier, W.G. Glasser, J. Adhes. 46 (1994) 165–180.
[25] G. Garnier, W.G. Glasser, Polym. Eng. Sci. 36 (1996) 885–894.
[26] M.A. Tshabalala, J. Appl. Polym. Sci. 55 (1997) 1013–1020.
[27] M. Kazayawoko, J.J. Balatinecz, M. Romansky, J. Colloid Interface Sci. 190 (1997) 408–415.
[28] D.J. Gardner, S.Q. Shi, W.T. Tze, Comparison of acid–base characterization techniques on lignocellulosic surfaces, in: Acid–base Interactions: Relevance to Adhesion Science and Technology, VSP, Utrecht, 2000, pp. 363–383.
[29] E. Papirer, E. Brendle, H. Balard, C. Vergelati, J. Adhes. Sci. Technol. 14 (2000) 321–337.
[30] J.M.R.C.A. Santos, M.H. Gil, A. Portugal, J.T. Guthrie, Cellulose 8 (2001) 217–224.
[31] J.Y.Y. Heng, D.F. Pearse, F. Thielmann, T. Lampke, A. Bismarck, Compos. Interfaces 14 (2007) 581–604.
[32] R.H. Mills, D.J. Gardner, R. Wimmer, J. Appl. Polym. Sci. 110 (2008) 3880–3888.
[33] P.R. Rani, S. Ramanaiah, K.S. Reddy, Surf. Interface Anal. 43 (2011) 683–688.
[34] E. Csiszár, E. Fekete, Langmuir 27 (2011) 8444–8450.
[35] N. Rjiba, M. Nardin, J.Y. Drean, R. Frydrych, J. Colloid Interface Sci. 314 (2007) 373–380.
[36] M.N. Belgacem, A. Blayo, A. Gandini, J. Colloid Interface Sci. 182 (1996) 431–436.
[37] E.L. Hult, P.T. Larsson, T. Iversen, Polymer 42 (2001) 3309–3314.
[38] V. Chunilall, T. Bush, P.T. Larsson, T. Iversen, A. Kindness, Holzforschung 64 (2010) 693–698.
[39] P. Rämänen, P.A. Penttilä, K. Svedström, S.L. Maunu, R. Serimaa, Cellulose 19 (2012) 901–912.
[40] J.R. Conder, C.L. Young, Physicochemical Measurement by Gas Chromatography, John Wiley and Sons, Chichester, England, 1979.
[41] H. Balard, D. Maafa, A. Santini, J.B. Donnet, J. Chromatogr. A 1198–1199 (2008) 173–180.
[42] F. Thielmann, J. Chromatogr. A 1037 (2004) 115–123.
[43] A.T. James, A.J.P. Martin, Biochem. J. (1952) 679–690.
[44] J. Schultz, L. Lavielle, C. Martin, J. Adhes. 23 (1987) 45–60.
[45] F.M. Fowkes, Ind. Eng. Chem. 56 (1964) 40–52.

[46] V. Gutmann, The Donor–Acceptor Approach to Molecular Interactions, Plenum Press, New York, 1978.
[47] F.M. Fowkes, J. Adhes. Sci. Technol. 4 (1990) 669–691.
[48] C. Saint-Flour, E. Papirer, Inid. Eng. Chem. Prod. Res. Dev. 21 (1982) 666–669.
[49] J. Schultz, L. Lavielle, Interfacial properties of carbon fiber–epoxy matrix composites. Inverse Gas Chromatography – Characterization of Polymers and Other Materials. American Chemical Society, Washington, DC, 1989.
[50] F.L. Riddle, F.M. Fowkes, J. Am. Chem. Soc. 112 (1990) 3259–3264.
[51] W.A. Zisman, Relationship of equilibrium contact angle to liquid and solid constitution, in: F.M. Fowkes (Ed.), Contact Angle, Wettability and Adhesion vol. 43, 1964, pp. 1–51.
[52] A.J. Svagan, M.A.S. Azizi Samir, L.A. Bergund, Adv. Mater. 20 (2008) 1263–1269.
[53] E.L. Quinn, J. Am. Chem. Soc. 49 (1927) 2704–2711.
[54] B. Wang, L.X. Huang, A.S. Mujumdar, Drying of nanosize products, in: A.S. Mujumdar (Ed.), Hankbook of Industrial Drying, third ed., CRC Press, New York, 2007, pp. 713–727.
[55] H. Montès, J.Y. Cavaillé, Polymer 40 (1999) 2649–2657.
[56] D. Meißner, J. Einfeldt, A. Kwasniewski, J. Non-Cryst. Solids 275 (2000) 199–209.
[57] V. Agarwal, G.W. Huber, W.C. Conner Jr., S. Auerbach, J. Chem. Phys. 135 (2011) 134506-1–134506-13.
[58] L. Awoyemi, T.O. Femi-Ola, Y. Aderibigbe, J. Indian Acad. Wood Sci. 7 (2010) 19–24.
[59] B.G. Rånby, Acta. Chem. Scand. 3 (1949) 649–650.
[60] P. Lu, Y. Hsieh, Carbohydr. Polym. 82 (2010) 329–336.